Numerical simulation of thermal conduction and diffusion through nanoporous superinsulating materials

Denis Rochais, Gilberto Domingues, Franck Enguehard

Numerical simulation of thermal conduction and diffusion through nanoporous superinsulating materials

D. Rochais (corresponding author), G. Domingues, F. Enguehard

CEA / Le Ripault, BP 16, 37260 Monts, France

Abstract

Nanoporous superinsulating materials have an extraordinary power of thermal insulation. The thermal conductivities of these heterogeneous materials can achieve a few $mW.m^{-1}.K^{-1}$ when they are placed under primary vacuum at ambient temperature. In this contribution, we focus on the numerical simulation of the conduction heat flux traveling through a nanoporous material in relation with its nanostructure. We have developed two models in order to study either steady-state conduction heat transfer or transient conduction heat transfer through a fractal representation of a nanoporous material, in order to determine either the effective thermal conductivity or the effective thermal diffusivity of the material. Then, we have applied these models to a study concerning the influence of the nanoparticle volume fraction on the effective thermal conductivity and the effective thermal diffusivity of a nanoporous material.

Key Words

Conduction heat transfer – Nanoporous materials – Thermal homogenization

Numerical simulation of thermal conduction and diffusion

through nanoporous superinsulating materials

D. Rochais (corresponding author), G. Domingues, F. Enguehard

CEA / Le Ripault, BP 16, 37260 Monts, France

1. Introduction

Nanoporous superinsulating materials (NSMs) are getting more and more attractive for various applications (particularly in the aerospace and construction industries) due to their extraordinary power of thermal insulation [1-5]. Indeed, their thermal conductivity falls down to a few $mW.m^{-1}.K^{-1}$ when they are placed under primary vacuum at ambient temperature. This value can be compared to the one of air (generally regarded as an excellent thermal insulator), equal to $25\ mW.m^{-1}.K^{-1}$ at ambient temperature and pressure.

Such a level of thermal insulation of NSMs finds its explanation in the microstructure of these materials. Very porous (their porosity is of the order of 90%) and made of extremely fragmented solid matter (the main solid constituents are generally brought down to nanometric scales), they force the conduction heat flux to travel through very tortuous routes made of a multitude of elementary thermal resistances located at the coalescences of neighboring nanoparticles. Furthermore, these NSMs include very small quantities of micrometric-scale fibers and particles. Whereas the fibers provide some mechanical reinforcement to the NSMs, the role of the particles, made of opaque materials in the [5µm – 80µm] infrared spectrum, is clearly to cut down the infrared thermal radiation transfer in the course of its progression within the nanoporous structures.

In this contribution, we want (i) to develop very simple models to quantify the level of conduction heat transfer traveling through a NSM in relation with its nanostructure, and then (ii) to use these models to study the impact of the nanoparticle volume fraction on the effective thermal conductivity and diffusivity of a NSM.

To this purpose, we will first describe in detail the micro and nanostructure of a typical NSM. Second, we will present the computer generation code that we use to construct our virtual NSM structures. Third, we will describe two models which allow us to perform either a steady-state thermal conduction numerical experiment or a time-resolved thermal diffusion numerical experiment. Finally, we will exploit these models to study the influence of the nanoparticle volume fraction on the effective thermal properties of a NSM.

2. Description of the structure of a typical NSM

As introduced previously, a NSM is typically made of (i) nanometric scale particles joined to one another to form a nanoporous matrix, the dominant constituent of the material in terms of volume fraction (near 100%), (ii) a small volume fraction (of the order of 1%) of micrometric scale particles expected to provide infrared opacity to the NSM, and (iii) a small volume fraction (of the order of 1%) of micrometric scale fibres for a mechanical reinforcement of the nanoporous structure. The nanoparticles, constituting the nanoporous matrix, form the dominant population in terms of solid volume fraction, therefore they must be made of a material that is a good thermal insulator. In a large majority of cases, this material is chosen to be amorphous silicon oxide a-SiO_2 .

Figure 1 is a TEM image at a micrometric scale (the surface covered by this image is approximately $30\,\mu m \times 40\,\mu m$) of a particular NSM made of a nanoporous a-SiO_2 matrix and of crystalline silicon carbide SiC microparticles: the nanoporous matrix appears as the grey

phase, whereas the SiC microparticles are the dark inclusions. We can suppose that the dispersed microparticles, in low volume fraction, contribute weakly to the conduction heat transfer.

Figure 1: TEM image at a micrometric scale of a particular NSM made of a nanoporous a-SiO_2 matrix and of crystalline SiC microparticles. The nanoporous matrix appears as the grey phase, whereas the SiC microparticles are the dark inclusions. The white zones, corresponding to holes, as well as the parallel scratches apparent on this image are due to sample preparation.

The matrix is extremely porous (its porosity is more than 90%), and a TEM observation focused on this matrix reveals its nanotexture, as shown in figure 2. This image being at a scale of the order of 100 nm (the surface covered by the image is approximately $1.8\,\mu m \times 2.2\,\mu m$), stacks of coalesced a-SiO_2 nanoparticles appear (dark structures) as well as the 3D nanostructure that they constitute. A further TEM analysis allows an approximate evaluation of (i) the average diameter of these a-SiO_2 particles (10 nm) and (ii) the average size of the pores (between 50 and 100 nm).

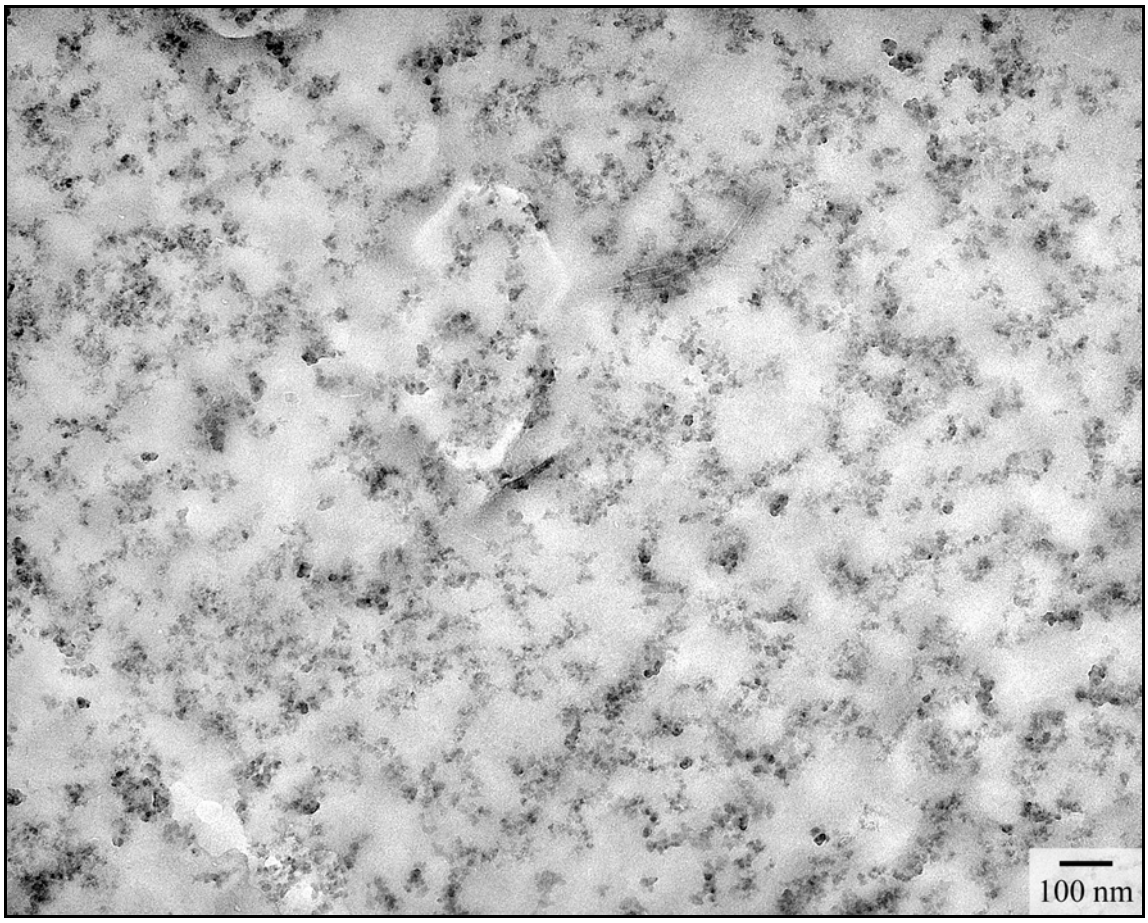

Figure 2: TEM image of the nanoporous a-SiO_2 matrix appearing in figure 1. Coalesced nanoparticle chains and stacks appear in dark and grey. The white zones correspond to the porosity.

A convection heat transfer cannot occur in such small pores [6]. Furthermore, the thermal conductivity of the confined fluid surrounding the nanoparticles is much lower than its thermal conductivity in an unconfined environment. Indeed, Griesinger *et al* [7] give the following correlation for the thermal conductivity of a confined gas:

$$\lambda_g(T, P, d) = \frac{\lambda_g^o(T)}{1 + 2\beta \frac{\bar{\ell}(T, P)}{d}} \tag{1}$$

where T is the temperature, P is the pressure, d is the pore size, $\overline{\ell}$ is the mean free path of the molecules, β is a dimensionless parameter depending on the nature of the gas and $\lambda_g^o(T)$ is the thermal conductivity of the gas in a unconfined state. For example, if we take $T = 300K$, $P = 1\,bar$ and $d = 100\,nm$, then we obtain $\lambda_g(T, P, d) \approx 6\,mW.m^{-1}.K^{-1}$ which is already smaller than the value of the thermal conductivity of air in a unconfined state: $\lambda_g^o(T) \approx 25\,mW.m^{-1}.K^{-1}$. Now, if the nanoporous matrix is placed under primary vacuum (for example at 1 mbar) at ambient temperature, then the confined gas thermal conductivity $\lambda_g(T, P, d)$ falls down to $6\,\mu W.m^{-1}.K^{-1}$: the gas becomes a nearly perfect insulating material. This participates of course to the insulating power of a NSM.

As described previously, a typical NSM can be regarded at 2 different characteristic scales: a micrometric one, where the material can be considered as a dispersed phase of micrometric scale particles and fibers embedded within a homogeneous matrix, and a nanometric one, where stacks and chains of coalesced nanoparticles appear. For each characteristic scale of the material, a particular strategy of conduction heat transfer modeling can be envisaged. At micrometric scale, classical homogenization laws (Maxwell-Garnett, Bruggeman …) can be used to calculate the NSM effective thermal conductivity, provided the microparticle volume fraction is small enough (which is the case here) and the thermal properties of the matrix and the microparticles are known. At nanometric scale, we have to develop a numerical model in order to analyze the conduction heat transfer within the 3D matrix structure. In the following, we will focus on these models which allow us to determine the effective thermal conductivity and diffusivity of the matrix.

3. Computer generation of a virtual nanoporous matrix

To be representative of the conduction heat transfer within a NSM, our simulations must take into account its real structure. We resort to computer generation to construct matrix structures by the location in space of solid spheres meant to represent the nanoparticles. We have started in this field with very simple periodic structures (square-shaped, diamond-shaped, brick-shaped …). Although these structures are far from realistic, many interesting results can be obtained from their study, such as the influence of the structure on the heat flux travel. We will illustrate this point in the 4th part of this paper. Here, in order to generate more realistic nanostructures, we propose to apply the fractal method [8].

In reference [9], Legrand explains that nanoporous structures can be regarded as elementary schemes reproduced in the 3 space directions according to a mass evolution law having the following form:

$$M(R) \propto R^{D_f} \tag{2}$$

where R is the radius of the sphere limiting the nanoporous structure, $M(R)$ is the mass within this sphere and D_f indicates the fractal dimension associated to the nanoporous structure.

The procedure adopted to generate the nanostructure is based on a cluster-cluster aggregation process the rules of which are the following [10]:

- disperse a set of nanoparticles randomly in space,
- move each nanoparticle or aggregate in a random direction,
- if the nanoparticle or aggregate hits a neighbor, both are stuck to each other and will subsequently be moved together,

- application of boundary conditions.

Although these rules are simplistic, they are sufficient to assure the physics of the model if relevant parameters (space dimension of the structure, rigid stick and simultaneous diffusion of aggregates) are respected. The fractal dimension expected for such a generating process is of the order of 1.4-1.8 in 2-D or 3-D spaces [11].

Figures 3 and 4 show nanostructures obtained *via* the scheme presented above. They confirm the expected 2-D and 3-D fractal dimensions as determined by Jullien [11].

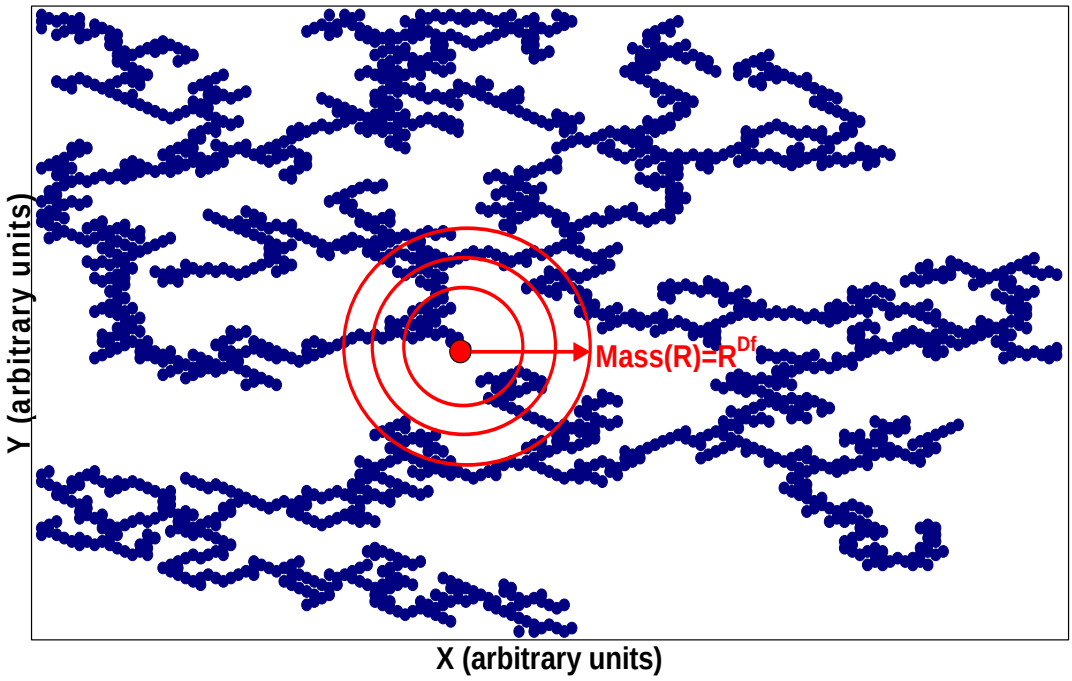

Figure 3: Representation of a nanoporous matrix as a 2-D fractal structure. The fractal dimension is 1.22 .

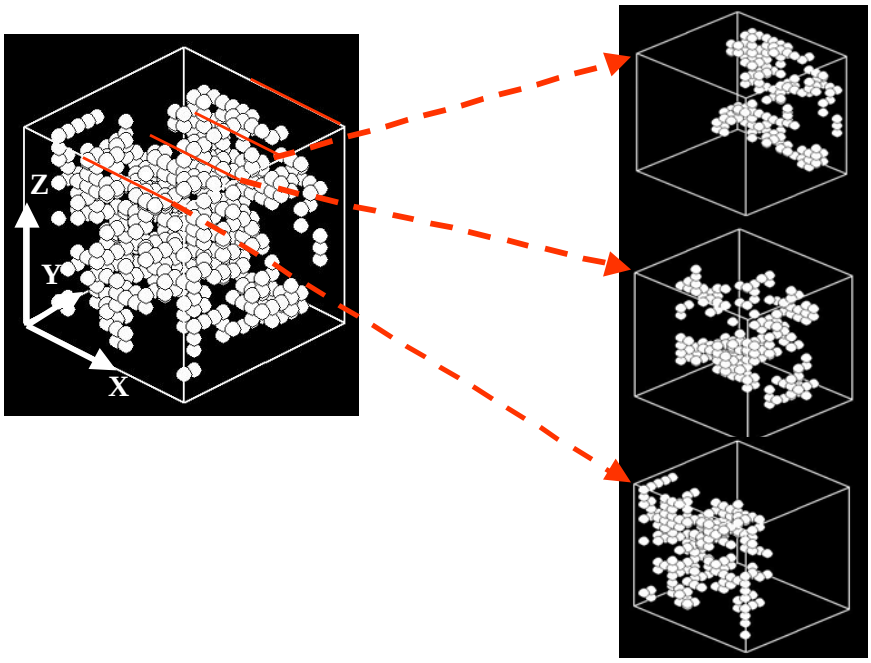

Figure 4: Representation of a nanoporous matrix as a 3-D fractal structure. The fractal dimension is 1.74 for a cubic box size of 150 nm. Cross-sections of the structure with 3 planes normal to the y axis are also presented.

4. Conduction heat transfer model

As discussed before, we want to study the conduction heat transfer traveling within a heterogeneous material made of nanoparticles surrounded by a gas, both constituents being assumed thermally isotropic. Two types of models will be developed: (i) a steady-state thermal conduction model to determine the effective thermal conductivity, (ii) a time-resolved thermal diffusion model to determine the effective thermal diffusivity and possibly other thermal properties.

4.1. Steady-state model

The knowledge (i) of the thermal conductivities of the 2 constituents of the matrix and (ii) of its spatial structure must allow us to determine the thermal conductivity tensor of its equivalent homogeneous material. This thermal homogenization step will be achieved with the help of a steady-state thermal conduction numerical experiment. A cube-shaped nanoporous structure is submitted to a temperature difference between 2 of its 6 boundary surfaces (see figure 5), its other 4 boundary surfaces being considered adiabatic. The conduction heat flux through the cube is evaluated, and from this quantity one can deduce the value of the effective thermal conductivity of the nanoporous structure in the direction of the imposed temperature difference.

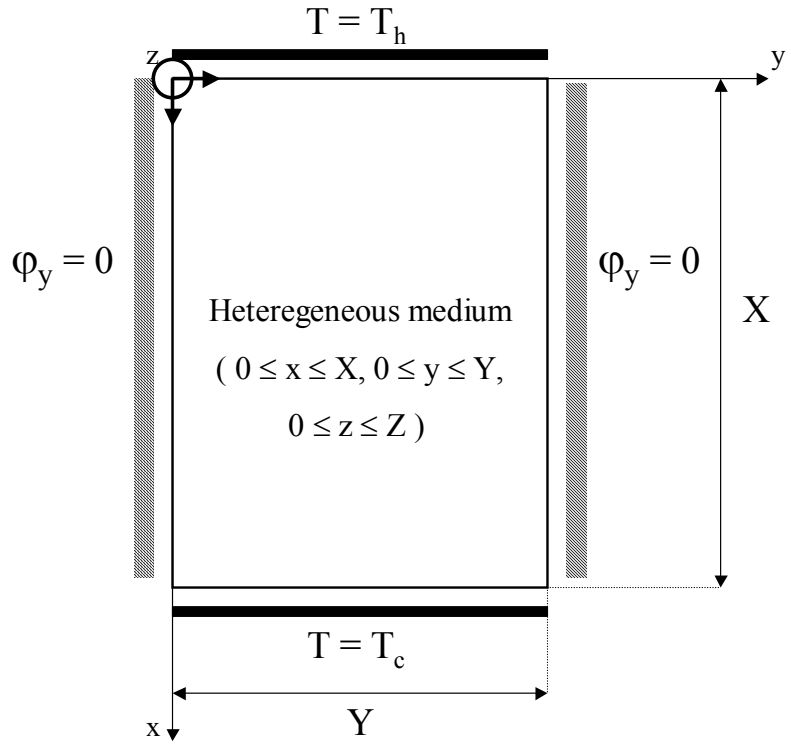

Figure 5: Schematic representation of the steady-state problem to be solved with its boundary conditions.

We have to solve the following 3-D steady-state thermal conduction problem within the heterogeneous sample:

$$\begin{cases} \vec{\nabla} \cdot \left(-\lambda \vec{\nabla} T \right) = 0 : \text{volume equation within the heterogeneous sample} \\ T = T_h : \text{imposed temperature at the "hot" boundary surface} \\ T = T_c : \text{imposed temperature at the "cold" boundary surface} \\ \vec{\varphi} \cdot \vec{n} = -\lambda \dfrac{\partial T}{\partial n} = 0 : \text{the other 4 boundary surfaces are considered adiabatic} \end{cases} \quad (3)$$

where $\vec{\varphi}$ is the heat flux $\left(\vec{\varphi} = -\lambda \vec{\nabla} T : \text{Fourier's law} \right)$ and $\vec{n}$ corresponds to the direction normal to the considered sample boundary surface. The thermal conductivity λ being not constant from a point to another within the matrix, we have to use a numerical technique to solve this problem. We have chosen a classical finite difference method to calculate the temperature field within the matrix. The considered material volume is discretized into elementary cubic elements. The mesh is made fine enough so that each element can be considered to be homogeneous and isotropic. Then, each element is attributed local thermal properties corresponding either to a nanoparticle or to the gas. The system of equations resulting from (3) is linear with a symmetric, positive definite matrix. A lot of numerical techniques exist that can achieve the matrix inversion. We have chosen a conjugate gradient one.

Once the temperature field is known, one can calculate the thermal power traveling through a plane section S parallel to the 2 imposed temperature boundary surfaces. This thermal power can be expressed by:

$$\Phi = \iint_S \vec{\varphi} \cdot \vec{n} \, dS \tag{4}$$

For example, in the case illustrated by figure 1, the expression (4) of the thermal power becomes:

$$\Phi = \iint_S \vec{\varphi} \cdot \vec{x} \, dS = \iint_S \varphi_x \, dS \tag{5}$$

where $\vec{x}$ is the unit vector normal to the considered section S.

Now, if we replace the heterogeneous material by its equivalent homogeneous material in the $\vec{x}$ direction, we can rewrite the expression of the thermal power Φ in the following way:

$$\Phi = \frac{\langle \lambda \rangle S}{X} \left(T_h - T_c \right) \tag{6}$$

where $\langle \lambda \rangle$ is the effective thermal conductivity of the heterogeneous material in the $\vec{x}$ direction and X is the distance between the 2 imposed temperature boundary surfaces.

Finally, eliminating Φ between (5) and (6), one reaches the following expression for the effective thermal conductivity $\langle \lambda \rangle$ in the $\vec{x}$ direction:

$$\langle \lambda \rangle = \frac{X}{S\left(T_h - T_c \right)} \iint_S \varphi_x \, dS = \frac{X}{S\left(T_h - T_c \right)} \iint_S \left(-\lambda \frac{\partial T}{\partial x} \right) dS \tag{7}$$

The numerical experiment described above, including the resolution of the temperature field, the calculation of the thermal power Φ (expression (5)) and finally the evaluation of the effective thermal conductivity $\langle\lambda\rangle$ (expression (7)), will have to be repeated in each space direction for the determination of the effective thermal conductivity tensor of the heterogeneous material.

To illustrate this approach, let us present results collected with periodic geometries. We have generated 3 very simple NSM matrix structures: a 2-D brick-shaped one, a 2-D diamond-shaped one, and a 3-D brick-shaped one. For these 3 material geometries, the porosity remains equal to 95%, the matrix is considered to be under vacuum (*i. e.* the thermal conductivity of the surrounding gas is taken to be 0), and the thermal conductivity of a nanoparticle λ_{np} is set equal to 1 $W.m^{-1}.K^{-1}$, corresponding to the bulk value for silica. We have solved the steady-state problem for each case and have calculated the resulting effective thermal conductivity of the matrix λ_m. Figure 6 shows the results: very interesting are (i) the orders of magnitude of the calculated effective thermal conductivities (they are comparable to the ones measured experimentally), (ii) the impact of the geometry on the value of the effective thermal conductivity (the 2-D diamond-shaped structure yields a λ_m value which is significantly lower than the one obtained with the 2-D brick-shaped structure), and (iii) the impact of the space dimension on the value of λ_m.

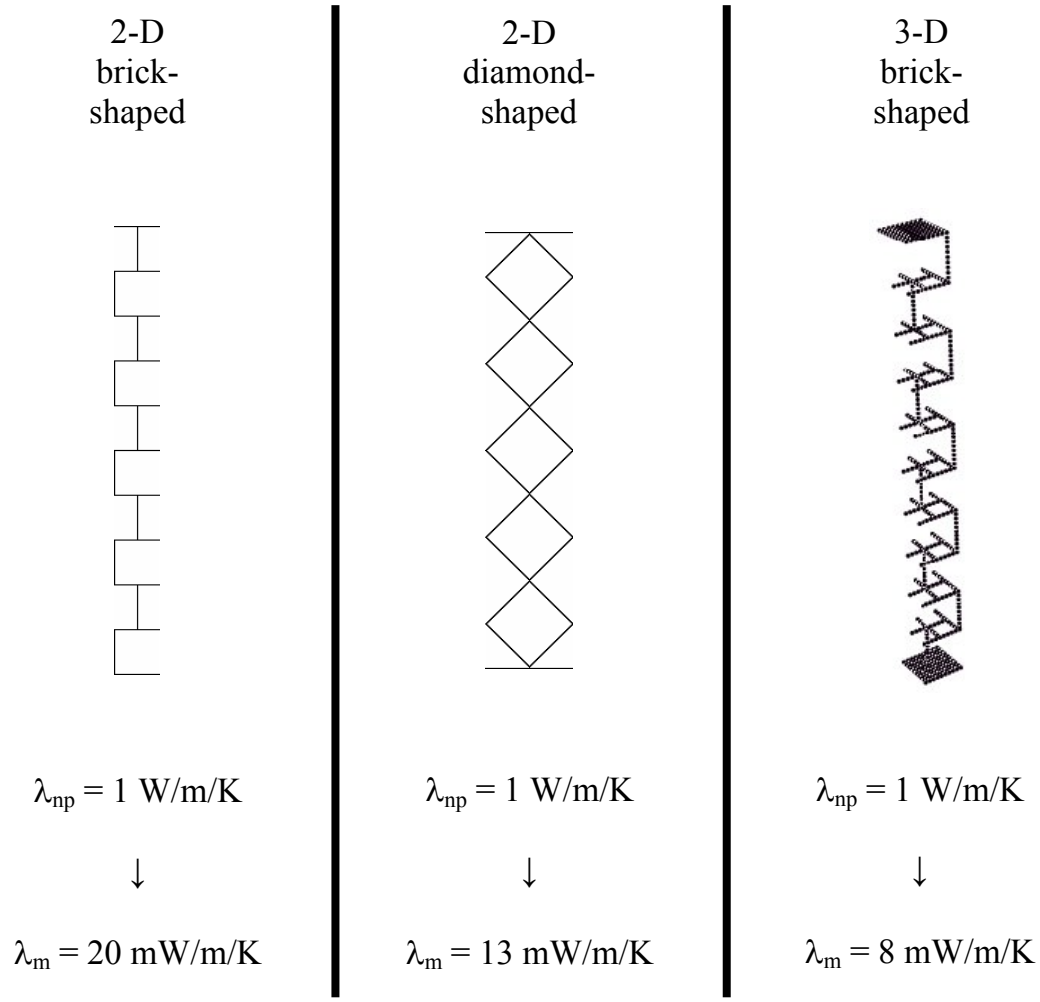

Figure 6: Comparison of the effective thermal conductivities calculated for 3 different nanoporous structures.

4.2. Time-resolved model

To study the thermal diffusion through a nanoporous matrix, we have developed a model inspired from a very classical thermal characterization technique, usually referred to as the "flash technique", for the experimental evaluation of the thermal diffusivity [12]. This time (see figure 7), the cube-shaped nanoporous structure is submitted to an instantaneous heat pulse on one boundary surface ($Q\,\delta(t)$ term), this boundary surface and the one located at its opposite are also submitted to permanent linearized heat losses (coefficient h, assumed

identical on the 2 surfaces), and the temperature elevation *versus* time curve is calculated on the boundary surface located at the opposite of the irradiated one. From this curve, it is possible to identify the effective thermal diffusivity of the heterogeneous material in the direction normal to the 2 boundary surfaces.

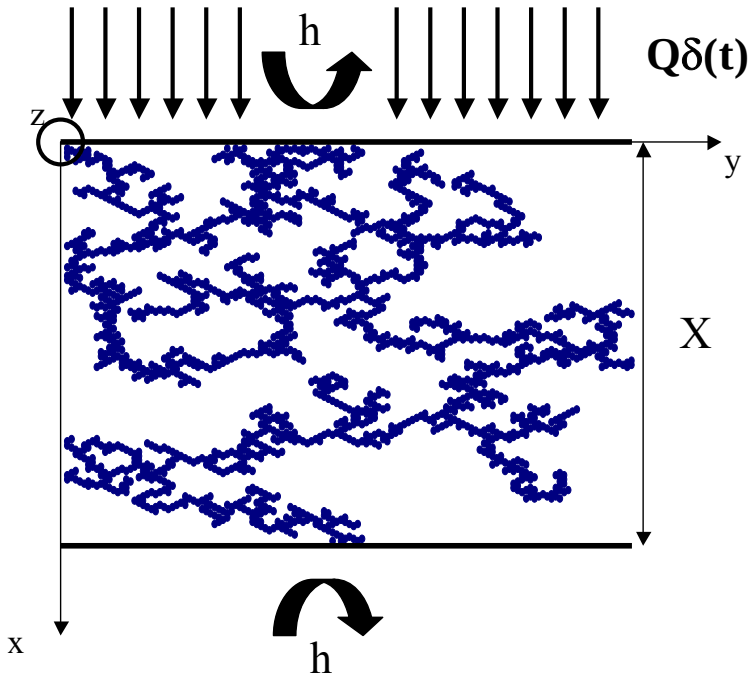

Figure 7: Schematic representation of the transient "flash" problem to be solved for the evaluation of the effective thermal diffusivity of a NSM.

What is the procedure? We have to solve the following 3-D transient thermal conduction problem through the heterogeneous material:

$$\begin{cases} C\dfrac{\partial T}{\partial t} = -\vec{\nabla}\cdot\left(-\lambda\,\vec{\nabla}T\right) : \text{volume equation within the heterogeneous sample} \\ T\left(t=0\right)=0 : \text{initial condition} \\ \vec{\varphi}\cdot\vec{n} = -\lambda\dfrac{\partial T}{\partial n} = -Q\,\delta(t) + h\,T : \text{boundary condition at the irradiated boundary surface} \\ \vec{\varphi}\cdot\vec{n} = -\lambda\dfrac{\partial T}{\partial n} = h\,T : \text{boundary condition at the opposite boundary surface} \\ \vec{\varphi}\cdot\vec{n} = -\lambda\dfrac{\partial T}{\partial n} = 0 : \text{the other 4 boundary surfaces are considered adiabatic} \end{cases} \quad (8)$$

where C is the volume specific heat (in $J.m^{-3}.K^{-1}$), Q is the energy per unit surface absorbed by the irradiated boundary surface (in $J.m^{-2}$), $\delta(t)$ is the Dirac delta function, and the notations n and $\vec{n}$ refer to the normal direction oriented outwards of the calculation domain.

A finite difference discretization scheme is applied to the system of equations (8), and the space and time resolved temperature field is calculated with the help of an implicit algorithm in time. At each time iteration, a linear system of equations is solved with the conjugate gradient algorithm. At the end of this procedure, an average temperature rise of the opposite boundary surface *versus* time curve is collected: this curve is called a thermogram.

Now, if we replace the heterogeneous sample by a homogeneous one of thermal conductivity λ, thermal diffusivity a and volume specific heat $C = \lambda / a$, then the analytical expression of the thermogram of the rear side of the sample is known:

$$T\left(x=X,t\right) = K\sum_{n=1}^{+\infty}\frac{\alpha_n \sin\alpha_n\left(\alpha_n^2+Bi^2\right)}{Bi\left(\alpha_n^2+Bi^2+2\,Bi\right)}\exp\left[-\frac{\alpha_n^2\,t}{\tau}\right] \quad (9)$$

where $K = Q/CX$ has units of temperature, $\tau = X^2/a$ is the thermal diffusion characteristic time, and $Bi = hX/\lambda$ is the dimensionless Biot number which indicates the level of the heat

exchange between the sample and its environment. Finally, the dimensionless coefficients α_n , $n \geq 1$ are the positive roots of the transcendental equation:

$$\tan \alpha = \frac{2\,\mathrm{Bi}\,\alpha}{\alpha^2 - \mathrm{Bi}^2} \tag{10}$$

It appears that expression (9) involves the time t plus the 3 parameters τ, Bi and K. In order to analyze experimental thermograms collected from homogeneous samples on our thermal diffusivity measurement "flash" setup, we have developed a least squares minimization routine that allows us to identify τ, Bi and K. The values of Bi and K can not be further exploited, because (i) the parameters Q and h of the experiment are not perfectly known, and (ii) the temperature rise curve on the rear side of the sample is not measured quantitatively. On the other hand, the knowledge of τ results in an immediate evaluation of the thermal diffusivity a of the sample *via* the relation:

$$a = \frac{X^2}{\tau} \tag{11}$$

When dealing with "numerical experiments", the situation is quite different because all quantities are known: the parameters Q and h are inputs of the calculation, and the thermogram on the opposite boundary surface is quantitatively evaluated. Then, the identification of τ, Bi and K from the "numerical" thermogram gives us the possibility to determine respectively the effective thermal diffusivity $\langle a \rangle$, the effective thermal conductivity $\langle \lambda \rangle$ and the effective volume specific heat $\langle C \rangle$ of the heterogeneous material *via* the following relations:

$$\langle a \rangle = \frac{X^2}{\tau} \quad , \quad \langle \lambda \rangle = \frac{h\,X}{Bi} \quad \text{and} \quad \langle C \rangle = \frac{Q}{K\,X} \tag{12}$$

To illustrate this approach, we have performed a "flash" numerical experiment in the z direction on the 3-D fractal NSM representation shown on figure 4. The sample thickness X was equal to 230 nm, the energy surface density Q was set equal to 1 $J.m^{-2}$, and the coefficient h was given the value of 10^4 $W.m^{-2}.K^{-1}$ (*i. e.* a very high value, in order to compensate for the very low value of the thickness X and hence to produce a Bi value of the order of unity). The matrix was considered to be under vacuum, and the thermal properties retained for a nanoparticle were the following: thermal conductivity 1 $W.m^{-1}.K^{-1}$, volume specific heat 2.94 10^5 $J.m^{-3}.K^{-1}$ (corresponding to the bulk value for silica). We have calculated the thermogram on the opposite boundary surface and identified the effective thermal diffusivity, thermal conductivity and volume specific heat of the 3-D fractal NSM representation. Figure 8 shows the resulting thermogram and its related fit: a good agreement is observed between the two curves, which is a first indication that the heterogeneous sample behaves as a homogeneous material in the course of this transient numerical experiment. The minimization procedure allows us to identify τ, Bi and K and to derive the values of $\langle a \rangle$, $\langle \lambda \rangle$ and $\langle C \rangle$. We have found: τ = 1.12 10^{-6} s, Bi = 0.93, K = 83.1, $\langle a \rangle$ = 4.72 10^{-8} $m^2.s^{-1}$, $\langle \lambda \rangle$ = 2.47 $mW.m^{-1}.K^{-1}$ and $\langle C \rangle$ = 5.23 10^4 $J.m^{-3}.K^{-1}$. At this point, it is interesting to note that the 3 identified thermophysical properties $\langle a \rangle$, $\langle \lambda \rangle$ and $\langle C \rangle$ perfectly verify the relation $\langle \lambda \rangle = \langle a \rangle \times \langle C \rangle$, which is a further indication that the heterogeneous sample responds as a homogeneous material to the transient numerical experiment applied to it.

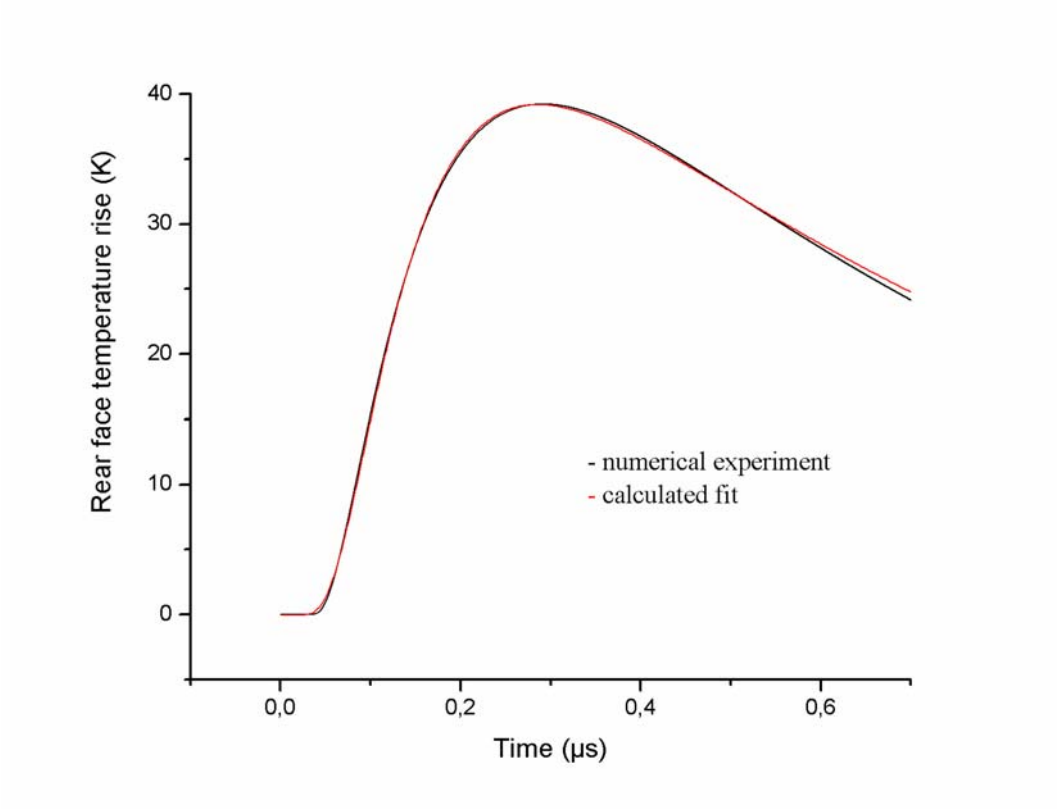

Figure 8: A numerical thermogram obtained with our transient model and its related fit.

To confirm the identified thermal conductivity value, we have performed a steady-state thermal conduction numerical experiment on the same material, with the same thermal conductivities and in the same heat flux traveling direction. The effective thermal conductivity value was found equal to 2.49 $mW.m^{-1}.K^{-1}$, which is very close to the one determined with the "flash" numerical experiment.

4.3. Application

The models presented above can reveal helpful for the analysis of *a priori* surprising experimental results. Thermal measurements made in our laboratory on NSMs of different densities indicated that the increase in the effective thermal diffusivity was small when the NSM density was multiplied by a factor of 2, and consequently that the effective thermal

conductivity behaved quasi-proportionally to the density. In order to validate these experimental observations, we have used our models to study the impact of the nanoparticle volume fraction on the effective thermal properties of the matrix. For this parametric study, we have chosen to simulate the heat transfer within a simple 3-D periodic brick-shaped structure (see figure 6), the nanoparticle volume fraction being easier to vary with this geometry than with a fractal structure. Figure 9 illustrates the effective thermal diffusivity evolution with the volume fraction as obtained *via* the time-resolved model, and figure 10 illustrates the effective thermal conductivity evolution with the volume fraction as obtained *via* the 2 models. These 2 graphs confirm our experimental characterizations: (i) the effective thermal diffusivity is multiplied by a factor of only 1.4 when the nanoparticle volume fraction is multiplied by a factor of 10, and (ii) the effective thermal conductivity evolves quasi-linearly with the nanoparticle volume fraction.

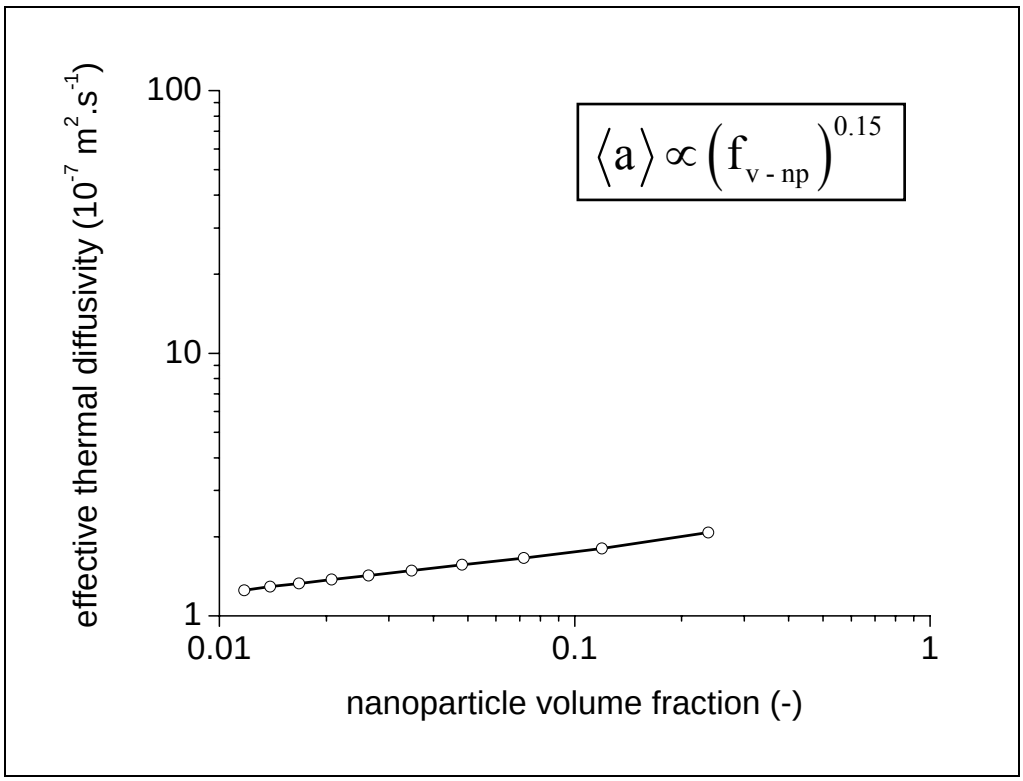

Figure 9: Effective thermal diffusivity variation *versus* the nanoparticle volume fraction.

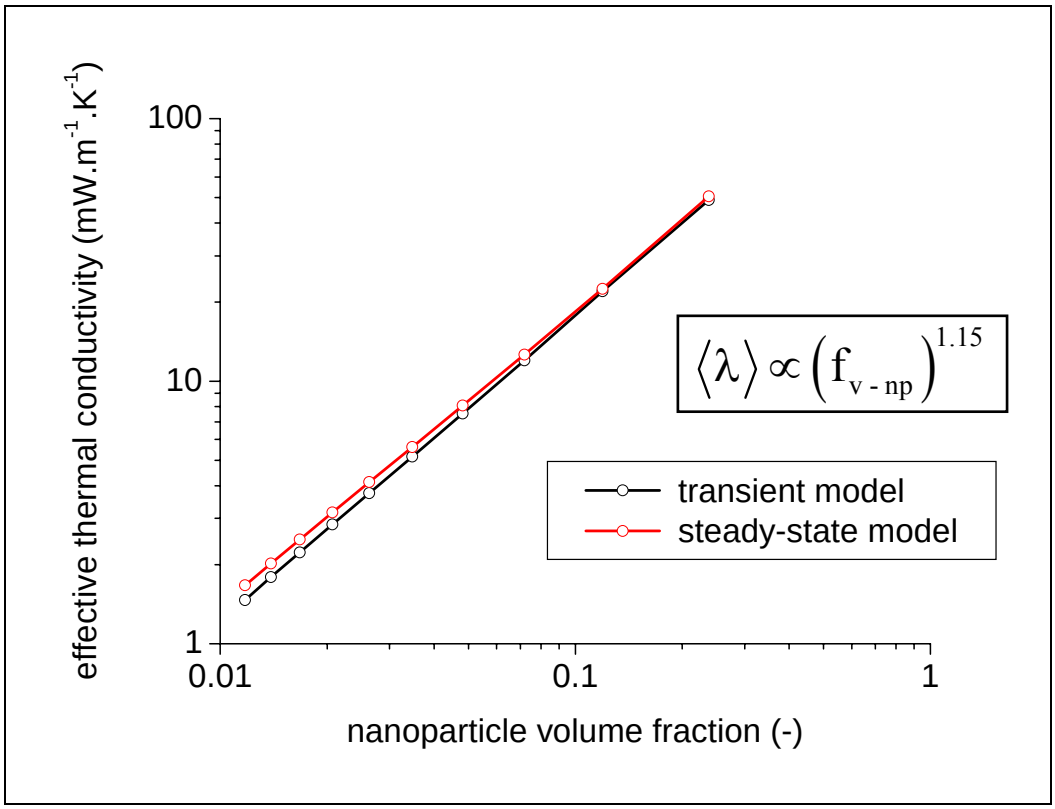

Figure 10: Effective thermal conductivity variation *versus* the nanoparticle volume fraction.

5. Conclusions

In this work, we have presented numerical models that allow us to quantify the level of conduction heat transfer traveling through NSMs. The first step of our simulations consists in the generation of a fractal representation of the matrix structure. Then, 2 types of simulations can be performed: either a steady-state thermal conduction numerical experiment, which allows us to calculate the effective thermal conductivity of the matrix, or a time-resolved thermal diffusion numerical experiment, which allows us to calculate the effective thermal diffusivity of the matrix as well as its effective thermal conductivity. These simple models have been applied to a study concerning the impact of the nanoparticle volume fraction on the effective thermal properties of a nanoporous matrix. The simulations have permitted to

understand the experimental results derived from "flash" measurements performed on NSMs of different densities.

For the moment, these models produce quite good approximations of the effective thermal properties of NSMs. Nevertheless, they need to be improved to integrate the specificities of heat transfer at the scale of a nanoparticle. Indeed, Domingues *et al* [13] have demonstrated that the heat transfer between 2 nanoparticles at a distance smaller than a nanoparticle diameter is 2 to 3 orders of magnitude more efficient than when they are in contact, which means that we need to ask ourselves about the separation between conduction and radiation at these length scales.

References

1. H. M. Strong, F. P. Bundy and H. P. Bovenkerk, *J. Appl. Phys.* **31**:39 (1960).
2. H. Bjurström, E. Karawacki and B. Carlsson, *Int. J. Heat Mass Transfer* **27**:2025 (1984).
3. D. W. Yarbrough, T. W. Tong and D. L. McElroy, *High Temp. Sci.* **19**:213 (1985).
4. P. Scheuerpflug, R. Caps, D. Buttner and J. Fricke, *Int. J. Heat Mass Transfer* **28**:2299 (1985).
5. C. Stark and J. Fricke, *Int. J. Heat Mass Transfer* **36**:617 (1993).
6. *Thermal transmission measurements of insulation*, edited by R. P. Tye (ASTM STP-660, 1978).
7. A. Griesinger, K. Spindler and E. Hahne, *Int. J. Heat Mass Transfer* **42**:4363 (1999).
8. B. M. Mandelbrot, *The fractal geometry of nature* (Freeman Press, San Francisco, 1982).
9. A. P. Legrand, *The surface properties of silicas* (Wiley, New York, 1998).
10. R. Jullien, *Phys. Rev. Lett.* **51**:1123 (1983).
11. R. Jullien, *J. Phys. A: Math. Gen.* **19**:2129 (1985).

12. W. J. Parker, R. J. Jenkins, C. P. Bulter and G. L. Abbott, *J. Appl. Phys.* **32**:1679 (1961).

13. G. Domingues, S. Volz, K. Joulain and J.-J. Greffet, *Phys. Rev. Lett.* **94**:1123 (2005).